1

Segmentation boosting with compensation methods in optical coherence tomography angiography images

Yih-Cherng Lee[1], Jian-Jiun Ding[1, *], Ling Yeung[2], Tay-Wey Lee[3], Chia-Jung Chang[4], Yu-Tze Lin[4], Ronald Y. Chang[5]

1 Graduate Institution of Communication Engineering, National Taiwan University, Taipei, Taiwan

2 Department of Ophthalmology, Keelung Chang Gung Memorial Hospital, Keelung, Taiwan and College of Medicine, Chang Gung University, Taoyuan, Taiwan

3 Biostatical Consultation Center, Keelung Chang Gung Memorial Hospital, Keelung, Taiwan

4 Department of Ophthalmology, Keelung Chang Gung Memorial Hospital, Keelung, Taiwan

5 Research Center for Information Technology Innovation, Academia Sinica, Taipei, Taiwan

* jjding@ntu.edu.tw

Abstract

Optical coherence tomography angiography is a noninvasive imaging modality to establish the diagnosis of retinal vascular diseases. However, angiography images are significantly interfered if patients jitter or blink. In this study, a novel retinal image analysis method to accurately detect blood vessels and compensate the effect of interference was proposed. We call this the patch U-Net compensation (PUC) system, which is based on the famous U-Net. Several techniques, including a better training mechanism, direction criteria, area criteria, gap criteria, and probability map criteria, have been proposed to improve its accuracy. Simulations show that the proposed PUC achieves much better performance than state-of-art methods.

Introduction

Retinal vasculature analysis is a critical subject in diagnosing and managing retinal vascular diseases. Optical coherence tomography angiography (OCTA) is an advanced rapid noninvasive method that can acquire the images for retinal vasculature analysis [1-4]. Chorioretinal vasculature contains a three-dimensional layered structure and it comprises a superficial layer, a deep layer, an outer retinal layer, and a choriocapillary layer. OCTA facilitates the detection of retinopathy [5], glaucoma [6], and diabetic complications [7]. However, OCTA images can be affected by human interference. For example, patients may blink unconsciously during OCTA infrared scanning. Therefore, it is common for an OCTA image to product several megascopic artifacts. Additionally, the vasculature sometimes tends to be rare, small, and thin due to some disease. These problems may degrade the quality of an OCTA image. In this study, we tried to solve the following two problems for OCTA image analysis:

  i) The image quality problem of noise-interfered blood vessels:

The noise may be caused by the environment, equipment, the vessel in the next layer, and small nerve fibers in the plexus. Additionally, as indicated previously, the

46   motion of a patient may produce flicker noise.

47   ii)   Disease problem:

48 In a healthy retinal image, vessels are evenly distributed on the retina. However, in
49 a diseased retinal image, severe vascular non-perfusion may occur. There are large
50 empty / black areas, making it difficult for a doctor to identify whether a cluster of
51 bright pixels in the dark region is indeed a vessel or an artifact.

52 Considering the above problems, some advanced noise filters and thresholding
53 methods have been proposed. For example, the adaptive thresholding methods
54 proposed in Phansalkar et al. [8] and Cole et al. [9] and the multiple enface image
55 averaging Uji et al. [10] were well-known methods for image intensity
56 enhancement. Moreover, to reduce the noise and enhance the visual ability of the
57 retina, in [11-18], several techniques were adopted, including the Gabor-filter-based
58 method [11], the Frangi-filter-based methods [12], the filter-bank-based architecture
59 [13, 17], the optically-oriented-flux [14] and thresholding [18]. In [15], the
60 compressive sensing method was applied to remove the noise of OCTA images. In
61 [16], the generalized Gauss-Markov random field and the guided bidirectional
62 graph search method were applied to perform retinal vessel segmentation in OCTA
63 images, respectively. However, these methods are not unsupervised and parameter-
64 sensitive and may produce unexpected noise by personal setting operations. In
65 recent years, with the fast development of deep learning, several learning-based
66 segmentation methods, including the convolutional neural network (CNN)-based
67 [19] and the U-Net-based methods [20, 21] have been proposed. These methods can
68 reproduce the curvilinear vessel shape for healthy retinas. However, when handling
69 diseased retinal images, there are some limitations and the performance is affected
70 by the artifact and the non-uniform distribution of vessels. Therefore, in this study,
71 we integrated the advantages of deep learning networks and conventional methods
72 and proposed the patch U-Net compensation (PUC) algorithm. The main concepts
73 of the proposed PUC algorithm are summarized as follows:

74   a)   To solve the vessel segmentation problem:

75 We modified the original U-Net model [20] by varying its training process to make
76 the model fit OCTA images perfectly. This modified U-Net model is treated as the
77 backbone of the proposed PUC algorithm. It can well identify the vessels with large
78 curvature.

79   b)   To solve the diseases retinal image problem:

80 We developed several techniques for artifact identification and vessel compensation
81 to address the problem well.

82 First, we proposed an artifact identification technique based on corner detection,
83 edge detection, and ridge detection [22]. A novel direction estimation method and
84 area thresholding method were adopted to identify whether a cluster of bright pixels
85 was a real noise or a small vessel. Its idea is based on human vision. It applies the
86 fact that the vessel should be ridge-like and fiber-like to distinguish the artifacts and
87 small vessels.

88

(a) Superficial layer　　　(b) Deep layer　　　(c) Outer retinal layer

(d) Choriocapillaris layer　　(e) Grid-based Vessel density of superficial layer　　(f) Red points are blood vessels
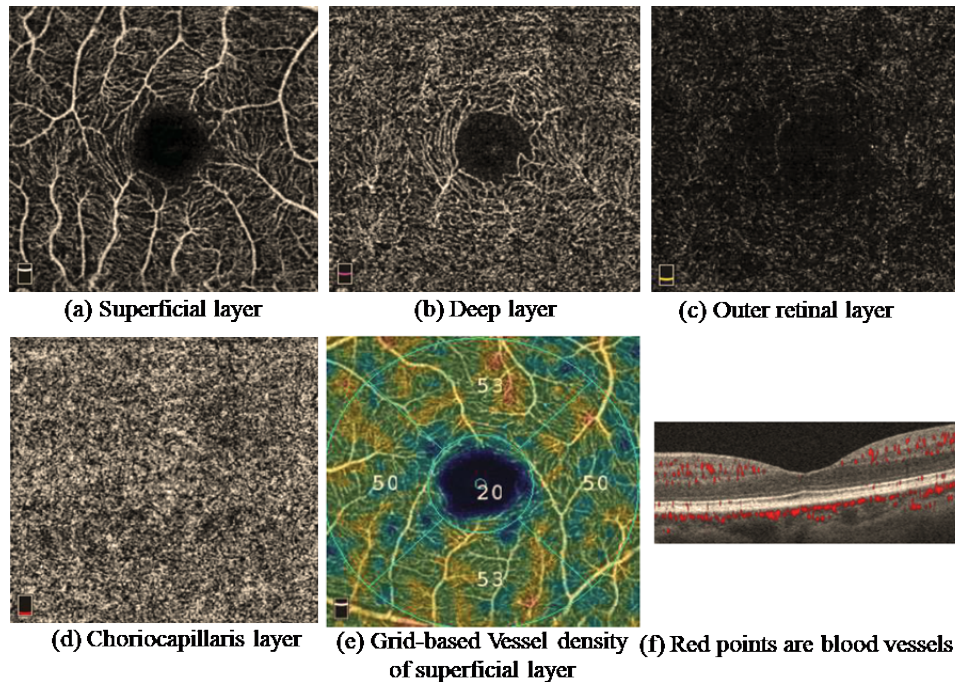
Fig 1. Outputs of the OCTA machine of RTVue XR 100 Avanti Edition, including (a)(b)(c)(d) four layers, (e) the vessel density map, and (f) cross-sectional images. The red points indicate vessels.
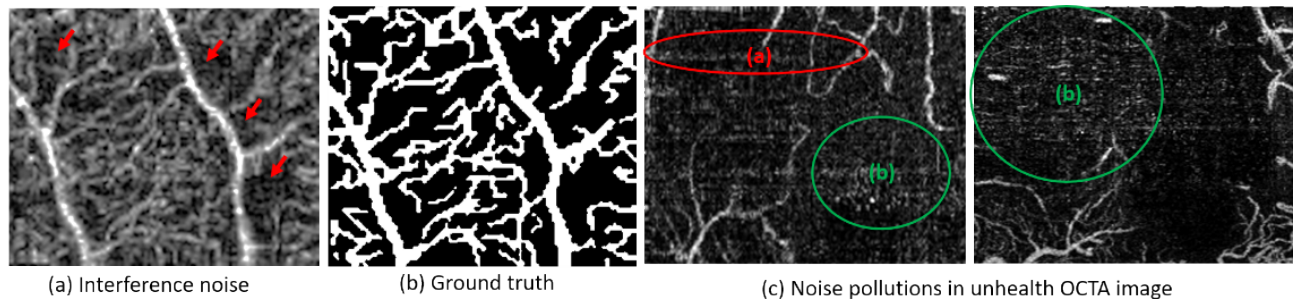

(a) Interference noise　　　(b) Ground truth　　　(c) Noise pollutions in unhealth OCTA image

Fig 2. (a) An OCTA raw image with noise (marked by red arrows); (b) the ground truth; (c) the scanning artifact problem (red ellipse) and noise (green ellipses) may be misidentified as vessels and affect the performance.

Subsequently, an adaptive compensation technique was applied to the remaining vessels. The U-Net [20, 21] performs vessel identification globally since its loss function is determined from whole pixels, not for the pixels in a special region. Therefore, we proposed a region-adaptive technique to connect small fragments in suspected regions to refine the output locally. These compensation techniques will be illustrated in detail in Sections "Compensation methods for noise reduction" and "Vessel compensation".

OCTA images and challenges in analysis

RTVue XR 100 Avanti Edition [23], which is an OCTA machine, provides the scanned images from the retina by the reflections on different vessels, as shown in Fig 1(f), to obtain four-layer information, as shown in Figs. 1(a)(b)(c)(d). Retina vessels are distributed like tree branches. Larger vessels (i.e. arterioles and venules) are mainly found in the superficial layer, while small vessels (capillaries) can be found in both superficial and deep layers. Vascular non-perfusion in superficial layer is an important feature of diagnosing and evaluating retinal vascular diseases.

Although OCTA machine may provide a vessel density map [24-27], as shown in Fig 1(e), the result is not robust to artifacts and noise, which may be misidentified as small vessels. How to filter the noise, like the red arrows, as shown in Fig 2(a), and retrieve the true vessels, as shown in Fig 2(b), is a challenging problem. Even when the patient moves the head slightly or blinks a little, noise is produced. Moreover, the scanning artifact problem may form a straight line in an OCTA image. It is often misidentified as a vessel. Consequently, it is insufficient to use only the intensity information to distinguish between vessels and noise. In particular, if the intensities of scanning artifacts are high and the vessels are blurred, using only the intensity information to identify vessels may cause several errors. Therefore, instead of applying some simple rules for vessel detection, a more sophisticated method is required.

In an OCTA image, if there is some bright region that is in fact not a vessel, then it is treated as noise. Due to machine oscillation and the motions of patients, most noise is either pepper-like or white-noise-like. Because the vessels, which are usually ridge-like, have several high-frequency components, it is suitable to apply the frequency-based filter (e.g., the lowpass filter) to remove the noise. Several studies [8-21] have been proposed to remove the bulk motion noise problems, as shown in Fig 2(a). However, it is still a challenge to deal with the strong artifacts and straight artifact lines, as shown in Fig 2(c).

In Fig 2(c), the red circles represent the strange thin straight line which comes from blink interference during the horizontal infrared scanning procedure and the green circle represents the noise interference from the OCTA machine. In this study, we used the direction criteria and the area criterion in Section "Compensation methods for noise reduction" to remove this type of noise.
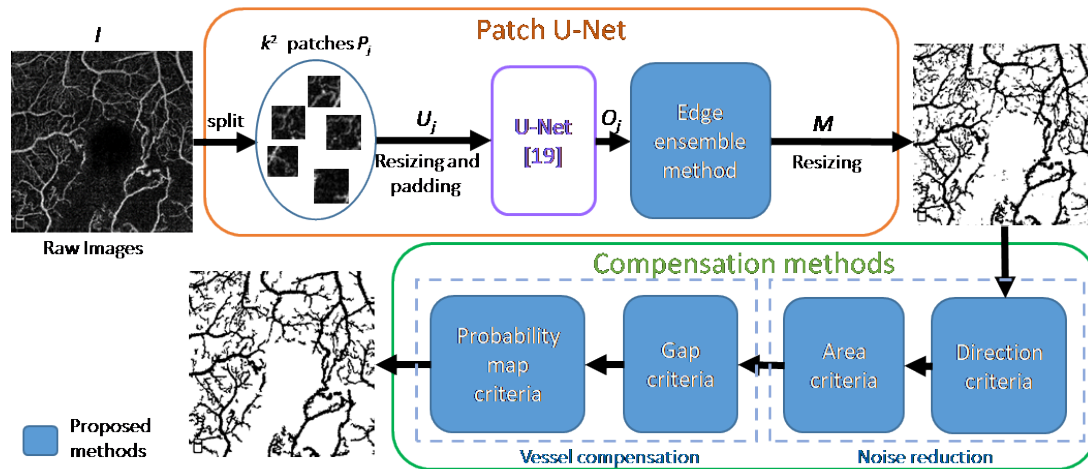
146

147 **Fig 3.** Architecture of the proposed PUC system.

148

(a) Raw images of two patches (b) Output images of patch U-Net
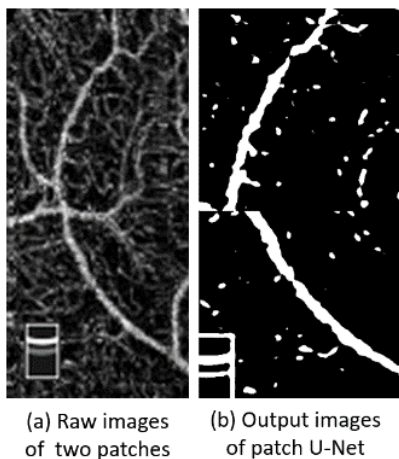
149

150 **Fig 4.** Illustration of the problem in the assembling process of the patch U-Net.

151

Materials and Methods

The U-Net, which is a multilayer deep learning model, has been applied in medical image processing [20, 21]. For example, in [20], the U-Net was applied to neuronal membrane image processing. However, OCTA images have denser vessel distributions and the noise interference problem is more severe in OCTA images than in other medical images. Therefore, in this study, we proposed an advanced method based on modifying the U-Net model to achieve a better vessel extraction result. The architecture of the proposed algorithm is plotted in Fig 3. It comprises two parts: (i) the patch U-Net and (ii) compensation methods.

Patch U-Net

The U-Net is widely used for segmentation. However, when we adopted it directly on OCTA images, the performance may be limited. If one feeds the original OCTA image into the U-Net directly, the training process may not be convergent to a good vessel detection result. Furthermore, taking the whole OCTA image may increase the use of the GPU memory. Because OCTA images are complicated and include several tiny vessels and artifact interferences, we found that using the U-Net directly could not describe the details of tiny vessels. Most of time, the model often ignores both tiny vessels and artifacts.

To deal with this problem, an interesting patch-based training strategy was proposed in this study. We also developed a meaningful and significant patch training strategy in OCTA image training on the U-Net-based model. We divided the input OCTA image into small and fixed size patches. Considering that the vessels in OCTA images were relatively small, using the proposed patch-based training strategy is very helpful for detecting tiny vessels successfully without increasing the effect of noise.

After obtained the outputs of the U-net for all patches, we fused these results. However, if one performs fusion directly, the discontinuous edge problem may occur at the boundaries of patches, as shown in Fig 4(b). Therefore, we proposed a patch ensemble method to address this issue. We applied the following methods to ensure that the output had continuous edges.

First, suppose that H is the input size of the U-Net, $\hat{H}$ is the output size of the U-Net, and $k \times k$ is the number of patches divided from the input image I. We padded each patch before network prediction to avoid the edge truncation effect. According to Algorithm 1, we generated, padded, and resized patches and used them as the inputs for U-Net training.

Second, we input a set of new patches U_j ($j = 1, 2, \ldots, k \times k$) to the U-Net model to acquire accurate output O_j ($j = 1, 2, \ldots, k \times k$) for the final ensemble procedure, as shown in Algorithm 2. Then, we resized the outputs and combined these by orders of Algrithom1 division orders.

The hyper-parameters are as follows: the input OCTA image size is $N = 304$, H is 572, $\hat{H}$ is 388, and $k = 4$. We divided the raw image into 16 uniform patches with size of 76×76. Then, each patch is symmetrically padded and treated as the input of the U-Net.

194

Algorithm 1: Generate Patches

Input: the square OCTA image I from dataset D where size(I) = $N{\times}N$
(default: the size of the U-Net input is H and size of the U-Net output is $\hat{H}$)

  1. **Divide** I into $k{\times}k$ patches P_1, P_2, …, $P_{k{\times}k}$ and each one has $\frac{N}{k}{\times}\frac{N}{k}$ pixels
  2. **For each patch** P_j
      a. **Perform symmetrically padding for** P_j:
         $$P(-\tau,n)=P(\tau,n), \qquad P(N/k-1+\tau,n)=P(N/k-1-\tau,n),$$
         $$P(m,-\tau)=P(m,\tau), \qquad P(m,N/k-1+\tau)=P(m,N/k-1-\tau),$$
         where $\tau = 1, 2, ..., d$ and $d = \dfrac{N}{k}\dfrac{H-\hat{H}}{2\hat{H}}$

      b. **Resize the patch to** $H{\times}H$ **pixels and obtain** U_j
Output: patches U_j (j = 1, 2, …, $k{\times}k$) and size(U_j) = $H{\times}H$.
          They will be treated as the inputs of the U-net.
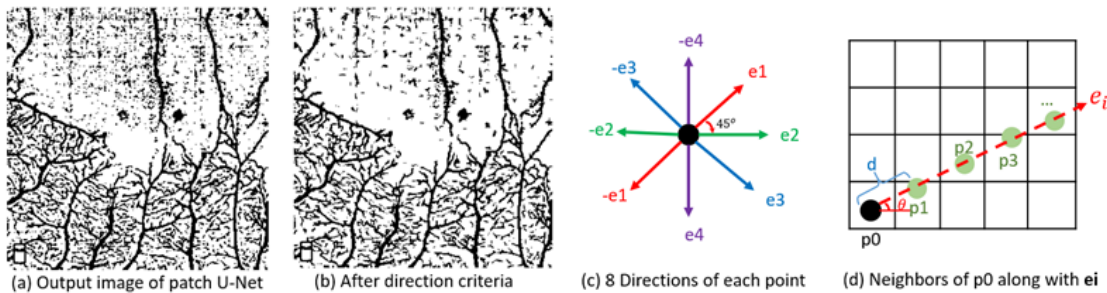

195

Algorithm 2: Patch Ensemble Methods

Input: O_j (j = 1, 2, …, $k{\times}k$) which are the outputs of the U-Net and size(O_j) = $\hat{H}{\times}\hat{H}$
  1. **Create an empty matrix** M **which has** $N{\times}N$ pixels
  2. **Resize each patch** O_j **to** $\frac{N}{k}{\times}\frac{N}{k}$ **pixels and obtain** T_j
  3. **Paste** T_j (j = 1, 2, …, $k{\times}k$) on the matrix M according to the orders that follow the division orders in Step 1 of Algorithm 1
Output: a predicted image M, which has $N{\times}N$ pixels
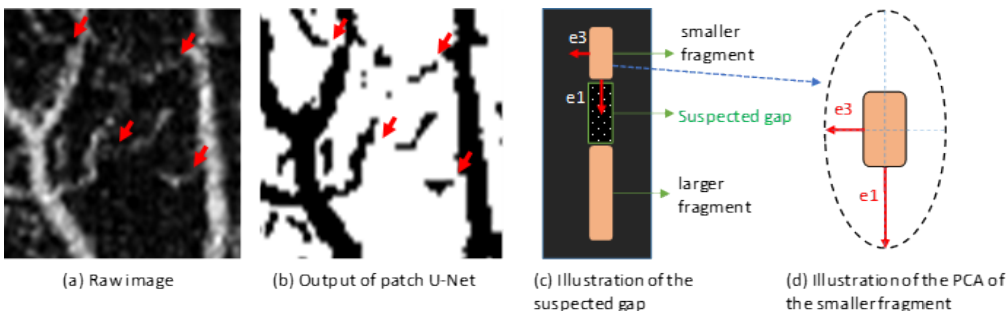

196

197   (a) Output image of patch U-Net   (b) After direction criteria   (c) 8 Directions of each point   (d) Neighbors of p0 along with **ei**

198   **Fig 5.** Illustration of the method of direction criteria.

199

    (a) Raw image   (b) Output of patch U-Net   (c) Illustration of the   (d) Illustration of the PCA of
                                             suspected gap   the smaller fragment

200
201   **Fig 6.** Illustrations of the gap criteria.

Compensation methods for noise reduction

After applying the patch U-Net to determine vessels from the retinal image, the output was compensated to distinguish between the noise and true vessels. The proposed compensation method comprises two parts: (a) the noise reduction part and (b) the vessel compensation part. The noise reduction part applies two methods, (i) direction criteria and (ii) area criteria, to refine the output of the patch U-Net model and remove the noise and artifact parts. The detail of the vessel compensation part will be described in Section "Vessel compensation".

i)   Direction criteria:

First, the output of the patch U-Net may contain some fragments and noise, as shown in Fig 5(a). We removed them according to their unique features. We can apply the techniques of feature point classification, which can classify a point into a peak, a ridge pixel, an edge pixel, a corner, or a flat pixel [22]. For each pixel, we observed the variations along the eight local directions, which were denoted by **e1**, -**e1**, **e2**, -**e2**, **e3**, -**e3**, **e4**, and -**e4**. To determine **e1**, first, we computed the convolution with the kernel matrix **K** and took the angle:

$$\theta_{m,n} = angle\left(U(m,n) * \mathbf{K}\right) - \frac{\pi}{2} = angle\left(\sum_x \sum_y U(m-x,n-y)K(x,y)\right) - \frac{\pi}{2} \tag{2}$$

where * means convolution, $U(m, n)$ is the output of the patch U-Net, and

$$K(x,y) = \frac{x + jy}{\sqrt{x^2 + y^2}} \quad \text{for } -3 < x, y < 3 \text{ and } (x, y) \neq (0, 0),$$

$K(x, y) = 0$ otherwise. Then, **e1** was determined from

$$\mathbf{e1} = \left(\cos\theta_{m,n}, \sin_{m,n}\right). \tag{3}$$

Note that **e1** varies with the location (m, n). Second, we performed clockwise rotation for **e1** with 45°, 90°, and 135° to produce **e2**, **e3**, and **e4**, respectively, as shown in Fig 5(c). Then, we computed the variations along the directions of $\pm$**e1**, $\pm$**e2**, $\pm$**e3**, and $\pm$**e4**, respectively. For example, to compute the variation along **e1** for pixel (x, y), we first set

$$p_t = U(m + t\cos\theta_{m,n}, n + t\sin\theta_{m,n}), \quad t = 0, 1, 2, 3. \tag{4}$$

If $m+t\cos\theta_{m,n}$ or $n+t\sin\theta_{m,n}$ is not an integer, then bilinear interpolation will be applied. Then, the variation along **e1** (denoted by V_1) was determined from the weighted sum of $p_n - p_0$:

$$V_1 = \sum_{t=1}^{3} w_t(p_t - p_0), \tag{5}$$

$$\text{where } w_t = \cos\left(\frac{\pi}{2}\left(\frac{t}{4}\right)\right), t = 1\sim3. \tag{6}$$

The variations along **e2**, **e3**, **e4**, −**e1**, −**e2**, −**e3**, and −**e4** (denoted by V_2, V_3, V_4, V_{-1}, V_{-2}, V_{-3}, and V_{-4}, respectively) can also be determined from Eq (4)-Eq (6) but $\theta_{m,n}$ in (4) is replaced by $\theta_{m,n} + k\pi/4$ where $k = 1, 2, 3, -4, -3, -2,$ and -1, respectively.

ii)   Area criteria

After denoising by the direction criteria, we tried to remove the artifacts. Different from noise, the artifact is not an isolated dot and cannot be removed by the direction criteria. However, we found that the artifact usually has a very small area. For a 304×304 image, if a region with an area smaller than 7 pixels, it could be absolutely defined as an artifact. Therefore, we use a well-known contour algorithm [28] to

243 determine all isolated regions and filter the regions whose area is less than 7 pixels.

244

Vessel compensation

246 In addition to noise and artifact removal, we also propose several techniques for
247 fragment connection. In a blurred OCTA image, sometimes some parts of the vessel
248 are not well detected and a vessel will be broken into several fragments in the
249 detection output. Because a vessel should have a line shape, after performing the
250 patch U-Net, it is appropriate to connect the two fragments that have a small gap, as
251 shown in Figs. 6(b)(c). Therefore, we proposed a geometric method to connect
252 vessel fragments.

253 iii) Gap criteria

254 If a group of segments in the detection result corresponds to the same vessel in the
255 ground truth, then they have line shapes and their directions and locations should be
256 similar to those of some surrounding fragments. By contrast, noise and artifact parts
257 are usually isolated dots. Although the noise from the scanning artifact also has a
258 line shape, it is very thin and too straight and can be well removed by the U-Net.
259 Therefore, we used the famous principal component analysis method to determine
260 the principal axis of the smaller fragment, as shown in Fig 6(d). The normalized
261 principle axis is denoted by **e1** and the direction orthogonal to **e1** is denoted by **e3**.
262 Then, we determined the line that could connect the end points of the two
263 fragments. If the projections of the line on **e1** and **e3** are α and β, respectively, and

$$\sqrt{\alpha^2 + (3\beta)^2} < threshold \qquad (7)$$

265 then the gap can possibly be a part of a vessel. In simulations, the threshold is
266 chosen as 8, which is 1/38 of the image width. We used 3β instead of β to ensure
267 that the connecting line had less projection on **e3**.

268 iv) Probability map criteria

269 However, if one connects two fragments according to only the length of the gap, it
270 is not enough to predict a more complicated association between two isolated
271 fragments. Therefore, we also adopt the possibility map acquired from the output of
272 the patch U-Net to determine whether two fragments should be connected. The
273 original U-Net architecture always uses a fixed threshold ($th = 0.5$) to conclude
274 whether a pixel belongs to the vessel or the background. However, it does not
275 consider the association with neighboring regions. In the proposed algorithm, we
276 adopted an adaptive threshold. For the gap between two fragments that satisfies Eq
277 (7), more attention should be paid and we lowered the threshold for the pixels
278 within the gap to make them easier to be identified as vessel pixels.

279 Moreover, for the non-gap part, the possibility map of the U-Net is also beneficial
280 for refining the vessel detection output. If $U(m, n)$ and $A(m, n)$ are the possibility
281 map of the U-Net and the intensity of the original OCTA image, respectively, when
282 $U(m, n) + A(m, n)/800 \geq th_{up} = 104/160$ then the pixel (m, n) is identified as a vessel
283 pixel. When $U(m, n) + A(m, n)/800 \leq th_{down} = 95/160$, (m, n) is identified as a
284 background pixel. If both the two inequalities are not satisfied, the criterion of $U(m, n) > 0.5$ is applied to determine whether a pixel is a vessel pixel.

Results

Database

Our database was obtained from the Chang Gung Memorial Hospital, Keelung, Taiwan. The study followed the tenets of the Declaration of Helsinki and it was approved by the Chang Gung Memorial Hospital Institutional Review Board. All OCTA images used in this study were the superficial layer of retinal vasculatures and had a size of 304×304. Half of the images were from eyes with retinopathy and others were from healthy cases. As a practical clinical scenario, most images in the database were interfered with by noise or artifacts. It comprises 42 raw OCTA images with 42 annotated ground truth, including 17 training images, 17 validation images, and 8 test images. For the training network, we also applied data augmentations (flipping horizontally or vertically and rotating in degrees [-45, 45]).

Evaluation

We use four metrics for evaluation: (i) accuracy, (ii) precision, (iii) recall (sensitivity), and (iv) the F1 score (Dice similarity coefficient). They are computed from the number of true-positive, true-negative, false-positive, and false-negative cases (denoted by TP, TN, FP, and FN, respectively):

$$\text{Precision} = \frac{TP}{TP + FP}, \qquad \text{Recall (Sensitivity)} = \frac{TP}{TP + FN}, \qquad \text{Accuracy} = \frac{TP + TN}{TP + TN + FP + FN},$$

$$\text{F1 Score (DICE coefficient)} = 2\frac{Recall \cdot Precision}{Recall + precision}. \tag{8}$$

Among these metrics, the F1 score takes both precision and recall into consideration and can well reflect the performance of an algorithm.

Experiments

In Table 1, we compare the proposed algorithm with several popular retinal vessel detection algorithms [11-14, 19, 21], including signal-processing-based methods [11, 12], traditional machine-learning-based methods [13, 14], and deep-learning-based methods [19, 21] associated with OCTA images. The results in Table 1 show that the proposed algorithm has a significantly better performance than the state-of-the-art methods. Compared to the study in [21], which is called the automated and network structure preserving segmentation (ANSPS) method, the F1 score of the proposed algorithm is 3.60% higher. Compared to other methods, the F1 score of the proposed algorithm is 5.17%-13.91 % higher.

Moreover, in Table 2, we conduct an ablation study. We test the performance of the proposed algorithm where (i) only the patch U-Net is adopted, (ii) direction criteria are adopted, (iii) direction + area criteria are adopted, (iv) direction + area + gap criteria are adopted, and (v) all the proposed techniques (the patch U-net and the direction + area + gap + probability map criteria) are applied. The results in Table 2 show that the proposed direction and area criteria are indeed beneficial in improving the performance of vessel detection, since they can remove noise and artifacts. However, if one applies the gap criteria alone without using the probability map criteria, the F1 score is decreased. If both the gap and the probability map criteria are applied, the F1 score can be significantly improved.

Table 1. Performance Comparison for Vessel Detection in Retinal OCTA Images

	F1 (DICE)	Precision	Recall	Accuracy
1. Multiscale [12]	0.7061	0.9382	0.5691	0.8973
2. Gabor [11]	0.7315	0.9661	0.5919	0.9073
3. Scird-ts [13]	0.784	0.7883	0.7877	0.9101
4. OOF[14]	0.7935	0.8411	0.76	0.9178
5. CNN [19]	0.7263	0.8344	0.6506	0.8973
6. ANSPS [21]	0.8092	0.7585	0.8835	0.9166
7. Proposed	**0.8452**	0.8541	0.8449	0.9344

Table 2. Ablation Study of the Proposed Algorithms

	F1 (DICE)	Precision	Recall	Accuracy
(i) PUN	0.7899	0.7128	0.9032	0.9028
(ii) PUN+DC	0.8315	0.793	0.8857	0.9244
(iii) PUN+DC +AC	0.8376	0.8258	0.8594	0.9286
(iv) PUN+DC +AC+GC	0.8313	0.8096	0.8648	0.9253
(v) PUN + DC + AC + GC + PMC (Our PUC system)	**0.8452**	0.8541	0.8449	0.9344

[1]PUN, patch U-Net, DC, direction criteria, AC, area criteria, GC, gap criteria, PMC, probability map criteria, PUC, patch U-Net compensation

Moreover, in Figs. 7 and 8, we perform a visual comparison of the proposed algorithm and other vessel detection algorithms. Compared to traditional signal processing methods and machine learning methods [11-14], the proposed algorithm can well retrieve the details of vessels. Even if the widths of the vessels are very small, they can be retrieved well by the proposed algorithm. Compared to the CNN-based method, when using the proposed algorithm, the small vessels can be well detected and the widths of the detected vessels match those in the ground truth. Compared to the ANSPS method [21], the proposed algorithm is more robust to the interference of noise and artifacts. Moreover, the connectivity of the detected vessels of the proposed algorithm is better than those of other algorithms.

In retinal OCTA image analysis, it is important to retrieve the details of vessels while avoiding noise interference. However, there is usually a tradeoff between the two goals. With the proposed algorithm, both the two goals can be well achieved and high-quality vessel detection results can be acquired.
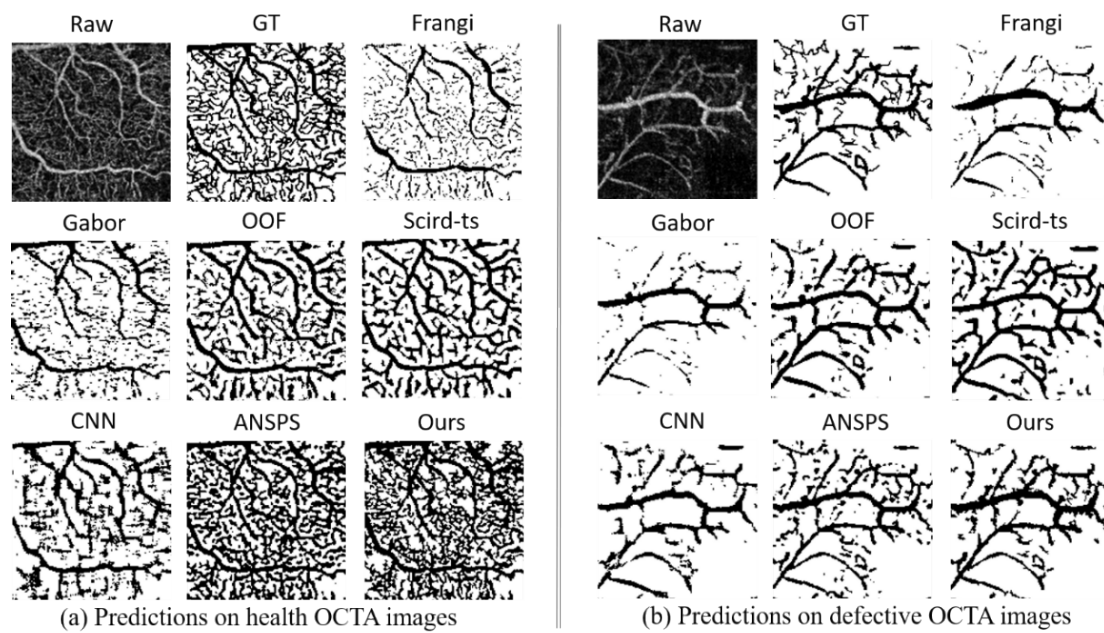
(a) Predictions on health OCTA images (b) Predictions on defective OCTA images

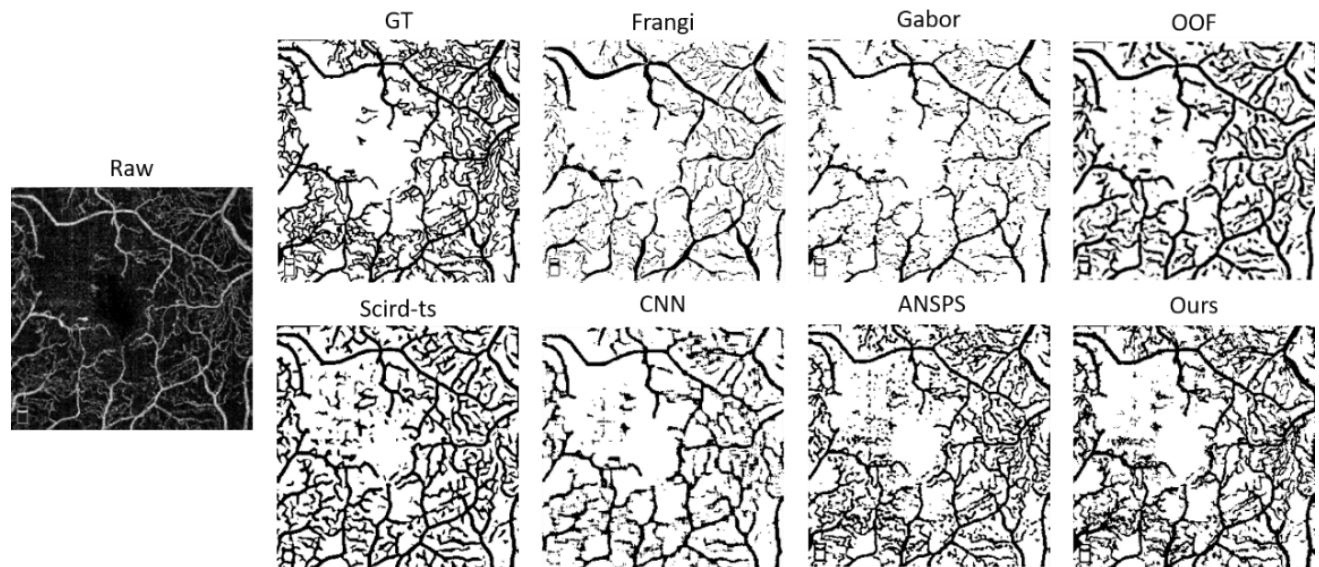**Fig 7.** Illustration of the method of direction criteria.

Fig 8. Illustrations of the gap criteria.

Conclusion

A novel PUC algorithm has been proposed for blood vessel detection on defective OCTA images. It adopts various techniques, including the deep learning architecture, the noise and artifact removal mechanism using the direction and area criteria, and the vessel compensation mechanism using the gap and probability map criteria. The proposed algorithm effectively compensates the disadvantages of learning-based methods and can well identify whether a small bright region is a true vessel or artifact. Through the proposed compensation method, we do not require a large amount of training data as regular CNN-based methods. The proposed algorithm can facilitate the evaluation of the vessel density and is beneficial for retinal diagnosis.

Acknowledgments

References

1. De Carlo TE, Romano A, Waheed NK, Duker JS. A review of optical coherence tomography angiography (OCTA). International journal of retina and vitreous. 2015; 1(1): 5.

2. Meleppat RK, Miller EB, Manna SK, Zhang P, Pugh Jr EN, Zawadzki RJ. Multiscale Hessian filtering for enhancement of OCT angiography images. In *Ophthalmic Technologies XXIX*. International Society for Optics and Photonics. 2019; 108581K

3. Jia Y, Bailey ST, Hwang TS, McClintic SM, Gao SS, Pennesi ME, Fujimoto JG. Quantitative optical coherence tomography angiography of vascular abnormalities in the living human eye. Proceedings of the National Academy of Sciences. 2015;112(18): E2395-E2402.

4. Kim AY, Chu Z, Shahidzadeh A, Wang RK, Puliafito CA, Kashani AH. Quantifying microvascular density and morphology in diabetic retinopathy using spectral-domain optical coherence tomography angiography. Investigative ophthalmology & visual science. 2016;57(9): OCT362-OCT370.

5. Walter T, Klein JC, Massin P, Erginay A. A contribution of image processing to the diagnosis of diabetic retinopathy-detection of exudates in color fundus images of the human retina. IEEE transactions on medical imaging. 2002;21(10):1236-1243.

6. Gopinath K, Sivaswamy J, Mansoori T. Automatic glaucoma assessment from angio-OCT images. In 2016 IEEE 13th International Symposium on Biomedical Imaging (ISBI). 2016 April: 193-196.

7. Matsunaga DR, Jack JY, De Koo LO, Ameri H, Puliafito CA, Kashani AH. Optical coherence tomography angiography of diabetic retinopathy in human subjects. Ophthalmic Surgery, Lasers and Imaging Retina. 2015;46(8): 796-805.

8. Phansalkar N, More S, Sabale A, Joshi M. Adaptive local thresholding for detection of nuclei in diversity stained cytology images. In 2011 International Conference on Communications and Signal Processing. 2011 February: 218-220.

9. Cole ED, Moult EM, Dang S, Choi W, Ploner SB, Lee B, Maier A. The definition, rationale, and effects of thresholding in OCT angiography. Ophthalmology Retina. 2017;1(5): 435-447.

10. Uji A, Balasubramanian S, Lei J, Baghdasaryan E, Al-Sheikh M, Borrelli E, Sadda S. R. Multiple enface image averaging for enhanced optical coherence tomography angiography imaging. Acta ophthalmologica. 2018;96(7): e820-e827.

11. Soares JV, Leandro JJ, Cesar RM, Jelinek HF, Cree MJ. Retinal vessel segmentation using the 2-D Gabor wavelet and supervised classification. IEEE Transactions on medical Imaging, 2006;25(9): 1214-1222.

12. Frangi AF, Niessen WJ, Vincken KL, Viergever MA. Multiscale vessel enhancement filtering. In International conference on medical image computing and computer-assisted intervention. 1998 October: 130-137.

13. Annunziata R, Trucco E. Accelerating convolutional sparse coding for curvilinear structures segmentation by refining SCIRD-TS filter banks. IEEE transactions on medical imaging. 2016;35(11): 2381-2392.

14. Law MW, Chung AC. Three dimensional curvilinear structure detection using optimally oriented flux. In European conference on computer vision. 2008 October: 368-382.

15. Husvogt L, Ploner S, Moult EM, Alibhai AY, Schottenhamml J, Duker JS, Maier AK. Using medical image reconstruction methods for denoising of OCTA data. Investigative Ophthalmology & Visual Science. 2019;60(9): 3096-3096.

16. Eladawi N, Elmogy M, Helmy O, Aboelfetouh A, Riad A, Sandhu H, El-Baz A. Automatic blood vessels segmentation based on different retinal maps from OCTA scans. Computers in biology and medicine. 2017;89: 150-161.

17. Oliveira WS, Teixeira JV, Ren TI, Cavalcanti GD, Sijbers J. Unsupervised retinal vessel segmentation using combined filters. PloS one. 2016;11(2): e0149943.

18. BahadarKhan K, A Khaliq A, Shahid M. A morphological hessian based approach for retinal blood vessels segmentation and denoising using region based otsu thresholding. PloS one. 2016;11(7): e0158996.

19. Prentašić P, Heisler M, Mammo Z, Lee S, Merkur A, Navajas E, Lončarić S. Segmentation of the foveal microvasculature using deep learning networks. Journal of biomedical optics. 2016;21(7): 075008.

20. Ronneberger O, Fischer P, Brox T. U-net: Convolutional networks for biomedical image segmentation. In International Conference on Medical image computing and computer-assisted intervention. 2015 October: 234-241.

21. Giarratano Y, Bianchi E, Gray C, Morris A, MacGillivray T, Dhillon B, Bernabeu MO. Automated and Network Structure Preserving Segmentation of Optical Coherence Tomography Angiograms. arXiv preprint. 2019; arXiv:1912.09978.

22. Pei SC, Ding JJ. New corner detection algorithm by tangent and vertical axes and case table. In IEEE International Conference on Image Processing. 2005 September: 1: I-365.

23. Holló G, Naghizadeh F. Influence of a new software version of the RTVue-100 optical coherence tomograph on the detection of glaucomatous structural progression. European Journal of Ophthalmology. 2015;25(5): 410-415.

24. Agemy SA, Scripsema NK, Shah CM, Chui T, Garcia PM, Lee JG, Rosen RB. Retinal vascular perfusion density mapping using optical coherence tomography angiography in normals and diabetic retinopathy patients. Retina. 2015;35(11): 2353-2363.

25. Kim AY, Chu Z, Shahidzadeh A, Wang RK, Puliafito CA, Kashani AH. Quantifying microvascular density and morphology in diabetic retinopathy using spectral-domain optical coherence tomography angiography. Investigative ophthalmology & visual science. 2016;57(9): OCT362-OCT370.

26. Guo Y, Hormel TT, Xiong H, Wang B, Camino A, Wang J, Jia Y. Development and validation of a deep learning algorithm for distinguishing the nonperfusion area from signal reduction artifacts on oct angiography. Biomedical optics express. 2019; 10(7): 3257-3268.

27. Nagasato D, Tabuchi H, Masumoto H, Enno H, Ishitobi N, Kameoka M, Mitamura, Y. Automated detection of a nonperfusion area caused by retinal vein occlusion in optical coherence tomography angiography images using deep learning. PloS one. 2019;14(11): e0223965.

28. Suzuki S. Topological structural analysis of digitized binary images by border following. Computer vision, graphics, and image processing. 1985;30(1): 32-46.